Additive Manufacturing: Metallurgy, Cut Analysis & Porosity

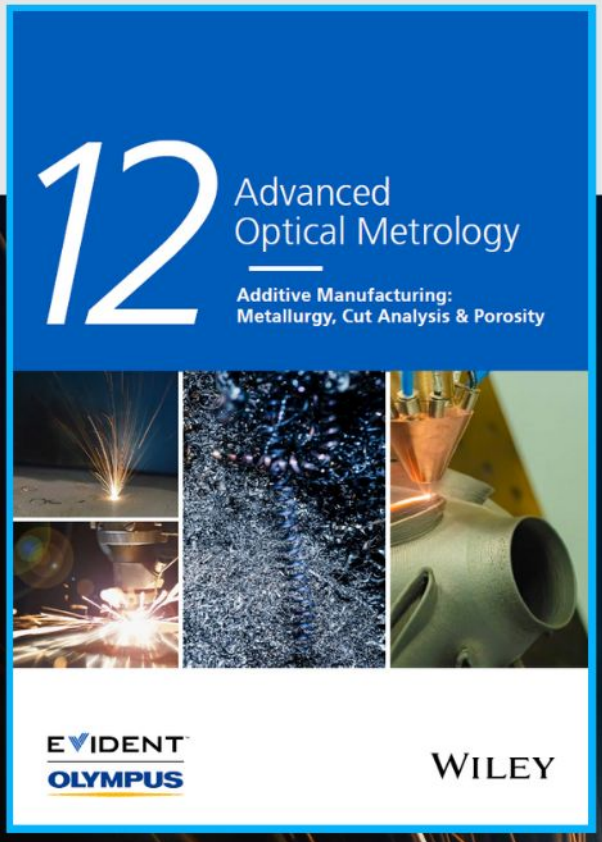

The latest eBook from Advanced Optical Metrology. Download for free.

In industry, sector after sector is moving away from conventional production methods to additive manufacturing, a technology that has been recommended for substantial research investment.

Download the latest eBook to read about the applications, trends, opportunities, and challenges around this process, and how it has been adapted to different industrial sectors.

EVIDENT
OLYMPUS

WILEY

ADVANCED FUNCTIONAL MATERIALS
www.afm-journal.de

Phthalocyanine Based Metal–Organic Framework Ultrathin Nanosheet for Efficient Photocathode toward Light-Assisted Li–CO_2 Battery

Jian-Hui Wang, Shan Li, Yifa Chen, Long-Zhang Dong, Ming Liu, Jing-Wen Shi, Shun-Li Li,* and Ya-Qian Lan**

Light-assisted Li–CO_2 battery, emerging as a powerful battery-technology to utilize light-energy, has attracted much attention yet it is still limited by the lack of efficient photocathode catalysts toward simultaneously promoted CO_2 activation/evolution processes. Here, a kind of phthalocyanine-based metal–organic framework nanosheet (CoPc–Mn–O) is prepared and applied as efficient photocathode catalyst in light-assisted Li–CO_2 battery. Thus-produced CoPc–Mn–O shows nanosheet-morphology (≈1 nm), dual active metal-sites (i.e., Co–N_4 and Mn–O_4), high conductivity, and photosensitivity. The resulting battery delivers a high round-trip efficiency of 98.5% with an ultralow voltage hysteresis of 0.05 V and superior cycling-stability (81.3%) for 60 h at 0.02 mA cm^{-2}, which is represented to be one of the best photocathodes to date. Density functional theory calculations and characterizations prove that the presence of photosensitive CoPc–Mn–O with dual active metal-sites endows an activation energy (3.2 eV) for CO_2 activation under light condition and simultaneously promote the CO_2 evolution to enhance the battery efficiency.

1. Introduction

With the continued consumption of fossil fuels and other non-renewable resources, the problem of inadequate energy supplies looms large and it is urgent to explore new alternative energy sources.[1–3] Rechargeable Li–CO_2 battery, possessing a high theoretical energy density of 1876 Wh kg^{-1} based on the reversible electrochemical reaction: 4Li + $3CO_2 \rightarrow 2Li_2CO_3$ +C (E_0 = 2.80 V vs Li^+/Li) and using CO_2 as the positive active medium, holds much potential in mitigating the growing greenhouse effect and providing energy supply.[4–7] However, the insulation characteristics of bulk Li_2CO_3 generated during the discharge/charge processes would lead to sluggish kinetics of CO_2 reduction reaction (CRR) and CO_2 evolution reaction (CER), eventually resulting in large voltage gaps and low energy density of Li–CO_2 battery.[8] Despite some promising strategies including cathode catalysts,[9–15] electrolyte additive,[16,17] or solid electrolyte[18–20] have been developed to address the challenging of Li–CO_2 battery, the achieved performances are still far from the criteria of practical applications and are restricted by the technique barriers by itself. To conquer the technique barriers, additional energy would be needed to assist and energy forms like light energy have been introduced into the battery system during past years, [21] thus developing the light-assisted Li–CO_2 battery.[22–25] Interestingly, some cathode catalysts such as SiC@RGO,[22] In_2S_3@CNT/SS,[23] CNT@C_3N_4[24] or TiO_2/CC,[25] have been developed and achieved promising properties, yet they still have drawbacks like: 1) most of them are based on semiconductors with light absorption ability under ultraviolet region (<5% in light energy); 2) the study of mechanisms especially for the electron–hole separation/transfer and light-assisted interactions are still rare and 3) most of them are mainly based on hybrid materials with nonporous or bulk forms, which are still hard to efficiently utilize the active sites and accurately modulate their structures. Therefore, it is urgent to elaborately design photosensitive cathode catalysts with wide absorption range, high porosity, well-tuned morphology and structures to simultaneously promote the light-assisted CRR and CER processes.

Metal–organic frameworks (MOFs), also known as porous coordination polymers (PCPs), are constructed from inorganic nodes (metal ions/clusters) and organic ligands through coordination bonds.[26] Since the 1990s, breakthrough progress has been made for MOFs and their potential applications have been widely explored in gas storage/separation,[27] sensing,[28] energy

Y. Chen, L.-Z. Dong, S.-L. Li, Y.-Q. Lan
National and Local Joint Engineering Research Center of MPTES in High Energy and Safety LIBs
Engineering Research Center of MTEES (Ministry of Education)
Key Lab. of ETESPG(GHEI)
School of Chemistry
South China Normal University
Guangzhou 510006, P. R. China
E-mail: chyf927821@163.com, 20200698@m.scnu.edu.cn; slli@njnu.edu.cn; yqlan@m.scnu.edu.cn
J.-H. Wang, S. Li, M. Liu, J.-W. Shi
School of Chemistry and Materials Science
Nanjing Normal University
Nanjing 210023, P. R. China
The ORCID identification number(s) for the author(s) of this article can be found under https://doi.org/10.1002/adfm.202210259.

DOI: 10.1002/adfm.202210259

storage/conversion,[29] biochemical fields,[30] etc. MOFs have many advantages, among which the most significant one is the tunability that can be specially designed through the rational selection of construction units to meet the desired demand of applications like Li–CO_2 battery. During past decades, only a few MOFs examples (e.g., Mn–MOF–74[31] and MnTPzP–Mn[32]) have been applied as the cathode catalysts and their applications are mostly restricted by the bottlenecks like low conductivity, lack of simultaneously demanded CRR and CER catalytic ability, insufficient for long-term stability, which generally result in high overpotential (mostly >1.0 V), low energy efficiency or cycling stability, etc. It seems that there exists a performance barrier for the design of MOFs as cathode catalysts through traditional battery techniques and thus extended strategies like light-assisted Li–CO_2 battery would be more desired to maximize the advantages of MOFs in this field. Nonetheless, the applications of MOFs in light-assisted Li–CO_2 battery have been rarely reported as far as we have known. Therefore, we intend to design and synthesize a kind of photosensitive MOFs based nanosheet assembling from phthalocyanine ligand with single Co–N_4 sites and Mn ions, and the corresponding considerations are as follows: 1) the conjugated structure of phthalocyanine molecule has wide and strong light absorption capacity;[33] 2) Co–N_4 sites in phthalocyanine or porphyrin functional groups has proven to be beneficial for the CRR processes, including CO_2 activation or Li_2CO_3 generation;[34,35] 3) Mn active sites in MOFs have also been studied with positive effect on the CER process[36–38] and 4) nanosheet morphology would expose more active sites to enhance the catalytic efficiency and is favorable for the electrode fabrication.[39] We suppose that the design of such powerful MOFs structures would be desired candidates to meet the demand of light-assisted Li–CO_2 battery, yet the exploration of them in this field is still challenging and rare to the best of our knowledge.

Herein, a kind of phthalocyanine-based MOF nanosheet (i.e., CoPc–Mn–O) has been synthesized through the construction of Co-phthalocyanine and Mn, which can serve as photocathode catalyst for light-assisted Li–CO_2 battery. The obtained CoPc–Mn–O presents ultrathin nanosheet morphology (thickness, ≈1 nm), high conductivity, dual active metal-sites (i.e., Co–N_4 and Mn–O_4 sites), and excellent photosensitivity, which is conducive to the CO_2 activation and evaluation processes. Specifically, CoPc–Mn–O based cell offers an ultra-low overpotential of 0.05 V with energy efficiency as high as 98.5% under full-spectrum conditions and can be rapidly discharged/charged at 0.02 mA cm^{-2} for 60 h. In addition, DFT calculations and sufficient characterizations show that the presence of photosensitive CoPc–Mn–O with dual active metal-sites are beneficial for both the CRR and CER processes under light condition. This work holds much promise in the exploration of porous crystalline materials for light-assisted battery techniques.

2. Results

The solvothermal reaction of CoPc–$(OH)_8$ and manganese (II) acetylacetonate at 85 °C gives a kind of microcrystalline powder of CoPc–Mn–O. As predicted, CoPc–Mn–O would be a 2D MOF constructed by CoPc–$(OH)_8$ ligands and the square-planar MnO_4 nodes (**Figure 1**a).[40] To prove it, the powder X-ray diffraction (PXRD) tests have been conducted. The result shows that CoPc–Mn–O has been successfully synthesized and its peak positions at 4.9, 9.7, and 27.5° belong to (110), (200) and (001) facets, respectively, which is consistent with its iso-reticular structures in the reported literatures (Figure 1b).[41] Furthermore, the Fourier infrared transform (FT-IR) test shows that –OH (1248 cm^{-1}) bond disappears and –C–O– (1266 cm^{-1}) bond appears when compared CoPc–Mn–O with the Co-phthalocyanine ligand (Figure S1, Supporting Information). The Co K side X-ray absorption near side structure spectrum (XANES) of CoPc–Mn–O shows that is similar to CoPc, indicating that their coordination environment is very close (Figure S2, Supporting Information). In addition, CoPc–Mn–O 's K-edge extended X-ray absorption fine structure (EXAFS) curve is similar to the profile of CoPc reference foil, but different from that of Co foil. These results show that the Co atoms of CoPc–Mn–O are located in the coordination geometry of the square plane (Figure 1c).[42] The Mn K-edge X-ray absorption near edge structure spectrum (XANES) of CoPc–Mn–O shows that it is located between Mn_2O_3 and MnO, indicating that its coordination environment is different from traditional oxides (Figure S2, Supporting Information). The presence of Mn–O bond can be seen from the K-edge extended X-ray absorption fine structure (EXAFS) curve of CoPc–Mn–O, further confirming the structure of the material (Figure 1c). In order to verify the valence state of metal in CoPc–Mn–O, X-ray photoelectron spectroscopy (XPS) test was carried out. XPS tests confirmed that Mn (II) maintained its original valence state, and the characteristic peaks for Mn $2p_{3/2}$ and Mn $2p_{1/2}$ are 641.3 and 653.4 eV, respectively (Figure S3, Supporting Information). Similarly, Co also maintains its bivalent state, the relative characteristic peaks were 781.0 and 796.5 eV for Co $2p_{3/2}$ and Co $2p_{1/2}$, respectively (Figure S3, Supporting Information).

In addition, transmission electron microscopy (TEM) test results show that the CoPc–Mn–O displays a kind of graphene-like nanosheet morphology with a width of ≈300 nm (Figure 1d). Specifically, the high-resolution TEM (HR-TEM) image of CoPc–Mn–O shows the clear lattice fringes, further confirming their long-range order structures (Figure 1d). In detail, the d-spacing of 0.35 nm corresponds well to the simulated interlayer distance of CoPc–Mn–O.[41] The nanosheet morphology is also supported by the atomic force microscope (AFM) tests, in which the thickness of CoPc–Mn–O is uniform over a large scale and the detected thickness is ≈1.25 nm (Figure 1e). Besides, the element energy dispersive spectroscopy (EDS) mapping exhibits the uniform distribution of N, Co, and Mn (Figure S4, Supporting Information).

In order to obtain a multifunctional photocathode with excellent electrical conductivity and flexibility, CoPc–Mn–O@rGO (CoPc–Mn–O loaded redox graphene) electrode material was obtained by using CoPc–Mn–O material and redox graphene (rGO) slurry as raw materials in a sand funnel device. The obtained electrode material has both the advantages and characteristics of the original CoPc–Mn–O and rGO. The surface morphology of CoPc–Mn–O@rGO was observed by using photo and SEM tests. As can be seen in Figure S5 (Supporting Information), the whole cathode is uniformly

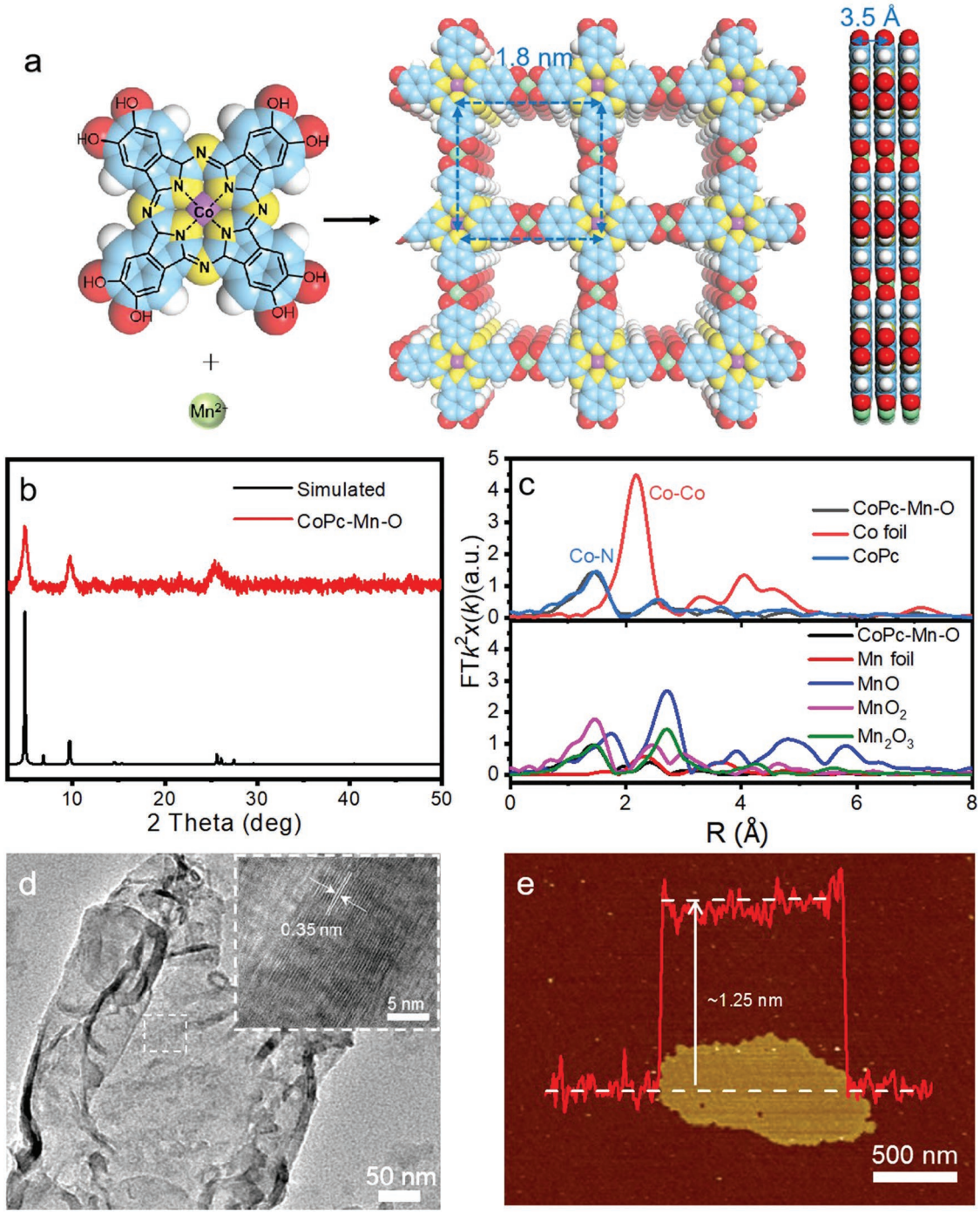

Figure 1. Characterization of CoPc–Mn–O. a) Design and synthetic scheme for CoPc–Mn–O. b) PXRD patterns. c) Synchrotron radiation patterns. d) TEM image of CoPc–Mn–O and the enlarged image of the circled place. e) AFM test.

distributed at macro level, and the material and graphene folds are interwoven. In order to confirm the relationship between r–GO and MOF materials more clearly, TEM tests were carried out. It can be seen from the Figure S6 (Supporting Information) that rGO is tightly layered with CoPc–Mn–O, which would be attributed to the both nanosheet morphology of them. The uniformity of CoPc–Mn–O in the electrode material can also be seen from the EDS mapping image, in which all of the elements are uniformly distributed over a large area (Figure S7, Supporting Information).

To facilitate the electrochemical property, the photocathode for light-assisted Li–CO_2 battery should possess a high effective utilization of the light across a wide spectrum as well as a low recombination rate for the photogenerated electron–hole

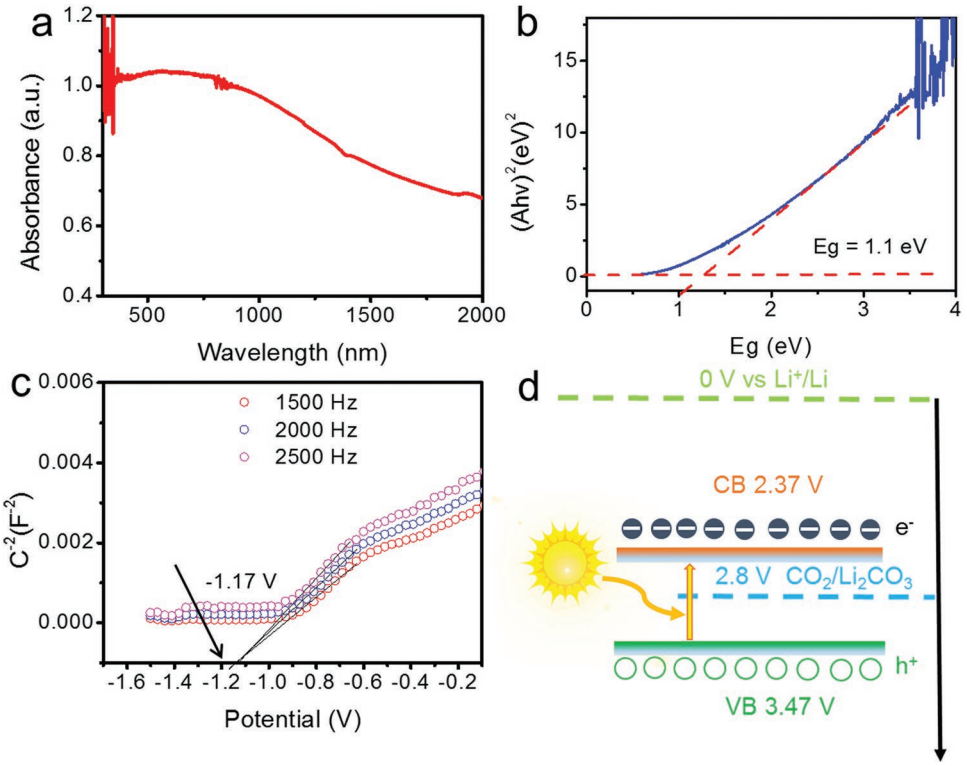

Figure 2. Spectral analysis of CoPc–Mn–O. a) UV–vis absorption spectra, b) The Tauc plot. c) Mott–Schottky plots. d) Energy diagram of CoPc–Mn–O and standard potential of CO_2/Li_2CO_3 versus Li^+/Li.

pairs. Therefore, the light-harvesting ability, carrier separation efficiency, and band structure of the sample were analyzed. The optical absorption properties of the CoPc–Mn–O were firstly evaluated via UV–vis absorption spectra (**Figure 2**a). The CoPc–Mn–O shows maximum adsorption edge of ≈2000 nm, which reveals a bandgap of 1.1 eV (Figure 2b). Moreover, the Mott-Schottky plot with a negative slope indicates the n-type semiconductor properties of CoPc–Mn–O (Figure 2c). The conduction band potential of the CoPc–Mn–O is estimated at 2.37 V versus Li^+/Li. Then, the valence band (VB) potential was calculated to be 3.47 V. As shown in Figure 2d, CoPc–Mn–O fulfills the essential condition of the light-promoted rechargeable Li–CO_2 battery that the redox potential of CO_2/Li_2CO_3 (2.80 V vs Li^+/Li) is located between the CB and VB potential. Thus, CoPc–Mn–O could fully utilize the photogenerated electrons and holes for solar energy conversion and storage, which would provide efficient light-assisted battery performance through the Li_2CO_3 oxidation. Based on the excellent performance of CoPc–Mn–O, the optical properties of CoPc–Mn–O@rGO have also been tested and showed remaining optical performance (Figure S8a, Supporting Information). According to the Tauc plot (Figure S8b, Supporting Information), the bandgap of CoPc–Mn–O@rGO is calculated to be 1.1 eV, which is consistent with that of CoPc–Mn–O. The CB and VB potentials of the CoPc–Mn–O@rGO are estimated at 2.34 and 3.44 V versus Li^+/Li, respectively (Figure S8c,d, Supporting Information). With the enhanced photoexcited charge separation in heterostructured CoPc–Mn–O@rGO, a higher reproducible ON–OFF photocurrent response generated in CoPc–Mn–O@rGO can be achieved than that of CoPc–Mn–O (Figure S9, Supporting Information).

To further investigate the effect of solar energy, LSV curves were measured in a CO_2-saturated 1.0 M LITFSI in TEGDME environment. Under illumination, both the onset potentials and the limiting current density of CoPc–Mn–O@rGO–L for CRR and CER are much higher than that without illumination in Figure S10 (Supporting Information). The cyclic voltammetry (CV) results further confirmed that the activity of the system was improved by light energy (Figure S11, Supporting Information). The excellent properties have been fully demonstrated and supported in Li–CO_2 battery performance tests. **Figure 3**a displays the discharge and charge curves of a Li–CO_2 battery in the dark and under illumination based on CoPc–Mn–O@rGO photoelectrode. Under illumination, the discharge platform of CoPc–Mn–O@rGO–L is up to 3.2 V, which is higher by 500 mV than that of CoPc–Mn–O@rGO (2.70 V) and even the theoretical potential of 2.80 V (Figure 3a). The CoPc–Mn–O@rGO–L based cell exhibits a lower charge voltage of 3.25 V than that of CoPc–Mn–O@rGO (4.07 V). Noteworthy, the achieved overpotential for CoPc–Mn–O@rGO–L based cell is as low as 0.05 V under light conditions, which is one of the best photocathode reported to date (Table S1, Supporting Information).

Figure 3b displays the rate capability at different current densities ranging from 0.01 to 0.2 mA cm^{-2}. The discharge voltages of CoPc–Mn–O@rGO–L are higher than those of CoPc–Mn–O@rGO counterparts over the entire current density range. Even at 0.2 mA cm^{-2}, the discharge voltage

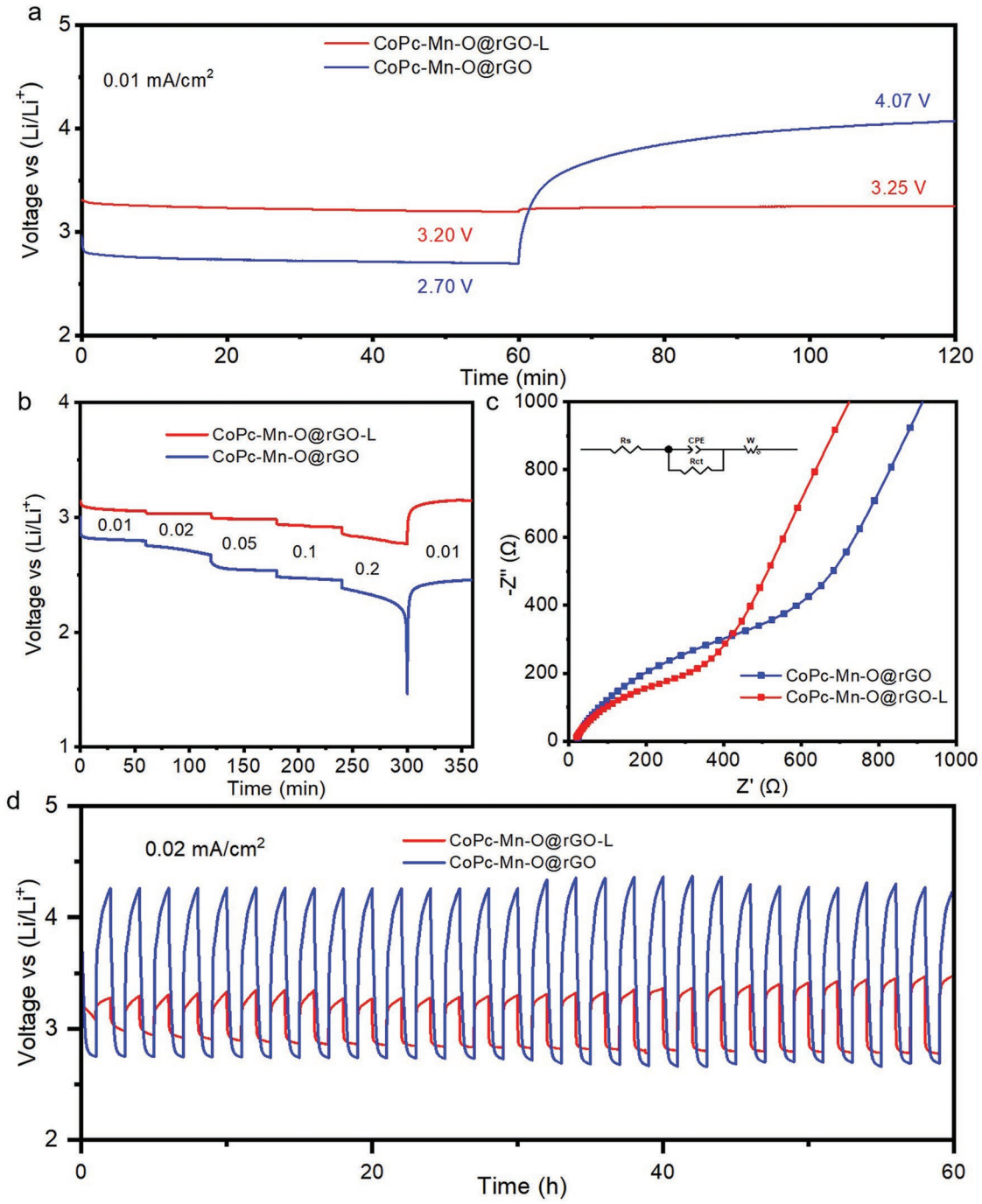

Figure 3. Battery performance of CoPc–Mn–O@rGO. a) Discharge and charge curves of the CoPc–Mn–O@rGO based Li–CO_2 battery with and without illumination at 0.01 mA cm^{-2}. b) Discharge voltage variation at different current densities (unit: mA cm^{-2}). c) EIS images. d) Voltage profiles of typical Li–CO_2 battery cycled with 0.01 mAh cm^{-2} cut-off capacity with and without illumination for CoPc–Mn–O@rGO–L and CoPc–Mn–O@rGO.

of CoPc–Mn–O@rGO–L (2.80 V) is still higher than that of CoPc–Mn–O@rGO (1.50 V). When the current density is reduced back to 0.01 mA cm^{-2}, the voltage returns to the similar value of the first cycle with light illumination, which cannot be completed without light (Figure 3b). These results demonstrate that light can boost the discharge performance of the Li–CO_2 battery. Electrochemical impedance spectra (EIS) have been implemented to analyze the superior rate performance (Figure 3c). The semicircle of CoPc–Mn–O@rGO–L is noticeably smaller than that of CoPc–Mn–O@rGO, demonstrating the more favorable charge transfer kinetics of CoPc–Mn–O@rGO–L. Moreover, the CoPc–Mn–O@rGO–L based battery still maintained good cycle stability at high current density, in which the overpotential remained low

at 0.02 mA cm^{-2} after 60 h (Figure 3d). These results indicate that the light energy indeed plays a vital role in improving the performances for both the discharge and charge processes.

Furthermore, various contrast samples have been prepared and tested to better demonstrate the superior performance. First, the blank rGO-based Li–CO_2 battery performance was tested. According to the test results shown in Figure S12 (Supporting Information), the battery performance has not improved after the illumination of light. In addition, the rGO–L based Li–CO_2 battery exhibits a higher discharge voltage of 2.81 V than that of rGO (1.85 V) and a lower charge voltage of 3.89 V than that with rGO (4.46 V). The results show that the presence of catalytic electrodes in both dark and light conditions greatly improved the performance of the battery, further demonstrating that light energy can be converted into electricity and help the whole process. However, its performance is far worse than that of CoPc–Mn–O@rGO–L, indicating the vital role of CoPc–Mn–O in improving the battery performance. In addition, the properties under light conditions of rGO-L based Li–CO_2 battery are almost the same as that of CoPc–Mn–O@rGO under dark conditions, which indicates that rGO mainly plays assisting role and has limited contribution to performance. Besides, CoPc@rGO has also been synthesized as contrast sample to test the battery performance under similar conditions. Under light condition, the CoPc@rGO–L based Li–CO_2 battery exhibits a higher discharge voltage of 2.99 V than that of CoPc@GO (2.70 V), which is still poorer than that of CoPc–Mn–O@rGO–L (Figure S13, Supporting Information). These results support the superiority of CoPc–Mn–O in promoting both CRR and CER processes to boost the performance of light-assisted Li–CO_2 battery.

Moreover, we have conducted a series of experiments to study the by-products during the discharge/charge processes. First, the discharge products were determined by the PXRD tests, and the main discharge products were Li_2CO_3 with or without light (Figure S14, Supporting Information). It can be seen that the crystallization peak of Li_2CO_3 appears after discharge, and the peak of Li_2CO_3 disappears after charge, which proves that the product can be effectively decomposed and is a reversible battery system for both with and without light conditions. At the same time, it can be observed from the PXRD pattern that although the discharge products belong to the same species with or without light, the crystallinity intensity is quite different. In the presence of light, the peak intensity of the product is weaker, and the peak of the product in the absence of light is obvious, which indicates that the lithium carbonate obtained in the presence of light may be more easily decomposed. Then, we carried out SEM characterization to evaluate the different battery stages. From the SEM images, it can be seen that the morphologies of the products are different for conditions with or without light. Under no-light conditions, the discharge products of the battery are rod-shaped with obvious edges and corners (size, ≈1 μm), resulting in limited contact surface with the electrode and low conductivity (**Figure 4**a). Under illumination, the morphology of the discharge products exhibits nanoflake morphology (size, ≈100 nm), in sharp contrast to the presence of no illumination (Figure 4b–d). This morphology would increase the contact area with the electrode, thereby increasing the catalytic activity and area, which is beneficial for the rapid decomposition of discharge products. Therefore, the light energy would facilitate the morphology tuning of discharge products and simultaneously promote electrode recovering to accomplish a fully reversible battery system.

To further reveal the role of CoPc-Mn-O in the light-assisted Li–CO_2 battery system and explore the possible mechanism, DFT calculations have been performed. In general, traditional Li–CO_2 battery contains two vital processes (i.e., CRR and CER processes), in which Co–N_4 and Mn–O_4 sites in MOFs have been proved to be beneficial for the CRR and CER processes in traditional Li–CO_2 batteries.[33–38] Based on the previously reported results and data detected in this work, we further carried out the theoretical calculations to study the catalytic effect of CoPc–Mn–O on this system. The DFT calculations show that the free energy change of the first step from CO_2 to *CO_2Li is 0.54 eV for the catalytic process by CoPc–Mn–O without light illumination, which can be assumed as the potential-determining step of the whole process (Figure 4f). Based on the electronic structure property analysis, it can be noted that the charge density of VBM and CBM locates mainly on the ligands of CoPc–Mn–O (Figure 4e), while the density states of CO_2 are in deep levels of the valence bands and conduction bands (Figure 4f). In that case, the activation process of the inert CO_2 is the first key step of the CO_2-conversion and the bandgap of CoPc–Mn–O only can barely meet the requirement. With light illumination, the photo-excited electrons with high energy can be first transferred to the Co sites, then relax to CO_2 to form CO_2^- (Figure 4f). Thereafter, the following conversion of CO_2 can be expected to be thermodynamically favorable process as the light provides multiple excited states with high energies. For the CER process, it still remains a daunting challenge in modeling the amorphous carbon as far as we know and the function of Mn–O_4 sites has been confirmed by the above-mentioned experimental results. Therefore, CoPc–Mn–O with bifunctional units are much beneficial for both CRR and CER processes in light-assisted Li–CO_2 battery, which endows high performance as certified by the various characterizations and DFT calculations.

3. Conclusion

In summary, we have prepared a kind of phthalocyanine MOF nanosheet (CoPc–Mn–O) and successfully explored its application as photocathode catalyst in light-assisted Li–CO_2 battery. Thus-obtained MOF nanosheet (thickness, ≈1 nm) exhibits high conductivity, dual active metal-sites (i.e., Co–N_4 and Mn–O_4 sites) and excellent photosensitivity, which is conducive to the CO_2 activation and evaluation processes. Noteworthy, the CoPc–Mn–O based cell offers an ultra-low overpotential of 0.05 V with energy efficiency as high as 98.5% under full-spectrum test conditions and can be rapidly discharged/charged at 0.02 mA cm^{-2} for 60 h. Moreover, DFT calculations and sufficient characterizations prove that the presence of photosensitive CoPc–Mn–O with dual active metal-sites are beneficial for both the CRR and CER processes

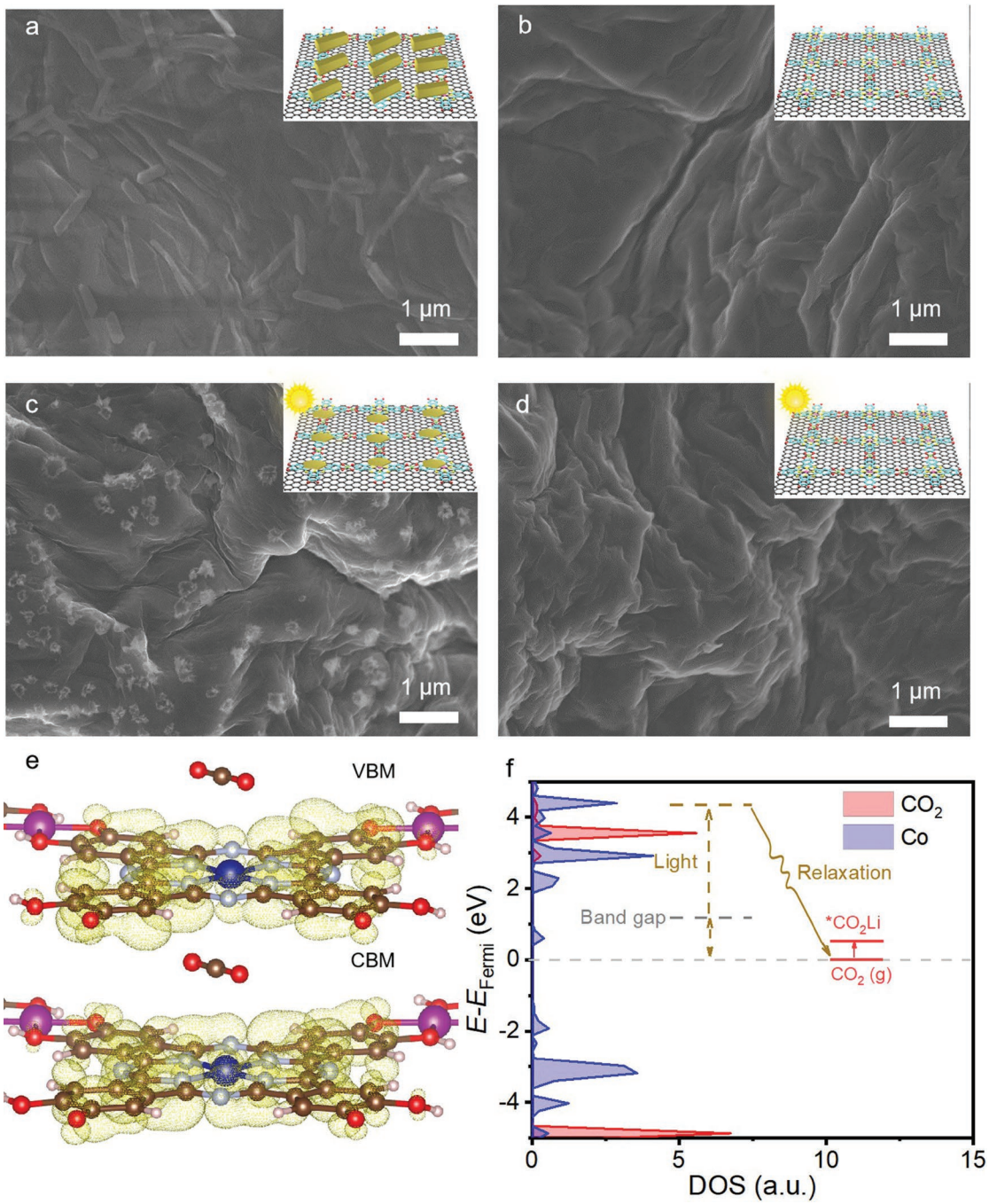

Figure 4. Characterization of discharge products and DFT calculations. a) SEM image of CoPc–Mn–O@rGO cathode after first discharge (insert is the schematic diagram). b) SEM image of CoPc–Mn–O@rGO cathode after first charge. c) SEM image of CoPc–Mn–O@rGO–L cathode after first discharge. d) SEM image of CoPc–Mn–O@rGO–L cathode after first charge. e) Projected charge density of the valence band maximum (VBM) and conduction band minimum (CBM) of CoPc–Mn–O. f) The density states of CoPc–Mn–O, red line denotes for CO_2 and blue line for Co.

under light condition. This work would extend the application scope of porous crystalline materials to light-assisted battery techniques.

Supporting Information

Supporting Information is available from the Wiley Online Library or from the author.

Acknowledgements

J.-H.W. and S.L. contributed equally to this work. This work was financially supported by the NSFC (Grants 22171139, 22225109, 21871141, 21871142, 21901122, and 22071109).

Conflict of Interest

The authors declare no conflict of interest.

Data Availability Statement

The data that support the findings of this study are available from the corresponding author upon reasonable request.

Keywords

Li–CO_2 batteries, light-assisted, nanosheets, phthalocyanine

Received: September 3, 2022
Revised: September 19, 2022
Published online:

[1] X. Mu, H. Pan, P. He, H. Zhou, *Adv. Mater.* **2020**, *32*, 1903790.
[2] J. Xie, Z. Zhou, Y. Wang, *Adv. Funct. Mater.* **2019**, *30*, 1908285.
[3] Z. Zhang, W.-L. Bai, K.-X. Wang, J.-S. Chen, *Energy Environ. Sci.* **2020**, *13*, 4717.
[4] X. Li, S. Yang, N. Feng, P. He, H. Zhou, *Chin. J. Catal.* **2016**, *37*, 1016.
[5] Y. Qiao, J. Yi, S. Wu, Y. Liu, S. Yang, P. He, H. Zhou, *Joule* **2017**, *1*, 359.
[6] A. Hu, C. Shu, C. Xu, R. Liang, J. Li, R. Zheng, M. Li, J. Long, *J. Mater. Chem. A* **2019**, *7*, 21605.
[7] Y. Jiao, J. Qin, H. M. K. Sari, D. Li, X. Li, X. Sun, *Energy Stor. Mater.* **2021**, *34*, 148.
[8] S. Yang, P. He, H. Zhou, *Energy Environ. Sci.* **2016**, *9*, 1650.
[9] Z. Zhang, Q. Zhang, Y. Chen, J. Bao, X. Zhou, Z. Xie, J. Wei, Z. Zhou, *Angew. Chem., Int. Ed.* **2015**, *54*, 6550;
[10] L. Qie, Y. Lin, J. W. Connell, J. Xu, L. Dai, *Angew. Chem., Int. Ed.* **2017**, *56*, 6970.
[11] S. Yang, Y. Qiao, P. He, Y. Liu, Z. Cheng, J.-j. Zhu, H. Zhou, *Energy Environ. Sci.* **2017**, *10*, 972.
[12] B. W. Zhang, Y. Jiao, D. L. Chao, C. Ye, Y. X. Wang, K. Davey, H. K. Liu, S. X. Dou, S. Z. Qiao, *Adv. Funct. Mater.* **2019**, *29*, 1904206.
[13] Y. Xing, Y. Yang, D. Li, M. Luo, N. Chen, Y. Ye, J. Qian, L. Li, D. Yang, F. Wu, R. Chen, S. Guo, *Adv. Mater.* **2018**, *30*, 1803124.
[14] X. Li, H. Wang, Z. Chen, H. S. Xu, W. Yu, C. Liu, X. Wang, K. Zhang, K. Xie, K. P. Loh, *Adv. Mater.* **2019**, *31*, 1905879.
[15] Y. Xing, K. Wang, N. Li, D. Su, W.-T. Wong, B. Huang, S. Guo, *Matter* **2020**, *2*, 1494.
[16] X.-G. Wang, C. Wang, Z. Xie, X. Zhang, Y. Chen, D. Wu, Z. Zhou, *ChemElectroChem* **2017**, *4*, 2145.
[17] W. Yin, A. Grimaud, I. Azcarate, C. Yang, J.-M. Tarascon, *J. Phys. Chem. C* **2018**, *122*, 6546.
[18] C. Li, Z. Guo, B. Yang, Y. Liu, Y. Wang, Y. Xia, *Angew. Chem., Int. Ed.* **2017**, *56*, 9126.
[19] X. Hu, Z. Li, J. Chen, *Angew. Chem., Int. Ed.* **2017**, *56*, 5785.
[20] R. Wang, X. Zhang, Y. Cai, Q. Nian, Z. Tao, J. Chen, *Nano Res.* **2019**, *12*, 2543.
[21] Q. Lv, Z. Zhu, S. Zhao, L. Wang, Q. Zhao, F. Li, L. A. Archer, J. Chen, *J. Am. Chem. Soc.* **2021**, *143*, 1941.
[22] Z. Li, M.-L. Li, X.-X. Wang, D.-H. Guan, W.-Q. Liu, J.-J. Xu, *J. Mater. Chem. A* **2020**, *8*, 14799.
[23] D. H. Guan, X. X. Wang, M. L. Li, F. Li, L. J. Zheng, X. L. Huang, J. J. Xu, *Angew. Chem., Int. Ed.* **2020**, *59*, 19518.
[24] X. X. Wang, D. H. Guan, F. Li, M. L. Li, L. J. Zheng, J. J. Xu, *Small* **2021**, *17*, 2100642.
[25] J. Li, K. Zhang, Y. Zhao, C. Wang, L. Wang, L. Wang, M. Liao, L. Ye, Y. Zhang, Y. Gao, B. Wang, H. Peng, *Angew. Chem., Int. Ed.* **2022**, *61*, e202114612.
[26] H. Li, M. Eddaoudi, M. O'Keeffe, O. M. Yaghi, *Nature* **1999**, *402*, 276.
[27] H. Li, L. Li, R.-B. Lin, W. Zhou, Z. Zhang, S. Xiang, B. Chen, *EnergyChem* **2019**, *1*, 100006.
[28] H. Yuan, N. Li, W. Fan, H. Cai, D. Zhao, *Adv. Sci.* **2022**, *9*, 2104374.
[29] H. Q. Xu, J. Hu, D. Wang, Z. Li, Q. Zhang, Y. Luo, S. H. Yu, H. L. Jiang, *J. Am. Chem. Soc.* **2015**, *137*, 13440.
[30] J. Tang, G. Tang, J. Niu, J. Yang, Z. Zhou, Y. Gao, X. Chen, Y. Tian, Y. Li, J. Li, Y. Cao, *J. Agric. Food. Chem.* **2021**, *69*, 2382.
[31] S. Li, Y. Dong, J. Zhou, Y. Liu, J. Wang, X. Gao, Y. Han, P. Qi, B. Wang, *Energy Environ. Sci.* **2018**, *11*, 1318.
[32] L.-Z. Dong, Y. Zhang, Y.-F. Lu, L. Zhang, X. Huang, J.-H. Wang, J. Liu, S.-L. Li, Y.-Q. Lan, *Chem. Commun.* **2021**, *57*, 8937.
[33] M. Lu, M. Zhang, C. G. Liu, J. Liu, L. J. Shang, M. Wang, J. N. Chang, S. L. Li, Y. Q. Lan, *Angew. Chem., Int. Ed.* **2021**, *60*, 4864.
[34] J. Chen, K. Zou, P. Ding, J. Deng, C. Zha, Y. Hu, X. Zhao, J. Wu, J. Fan, Y. Li, *Adv. Mater.* **2019**, *31*, 1805484.
[35] M. Goodarzi, F. Nazari, F. Illas, *J. Phys. Chem. C* **2018**, *122*, 25776.
[36] W. Ma, S. Lu, X. Lei, X. Liu, Y. Ding, *J. Mater. Chem. A* **2018**, *6*, 20829.
[37] S. Li, Y. Liu, J. Zhou, S. Hong, Y. Dong, J. Wang, X. Gao, P. Qi, Y. Han, B. Wang, *Energy Environ. Sci.* **2019**, *12*, 1046.
[38] Y. Mao, C. Tang, Z. Tang, J. Xie, Z. Chen, J. Tu, G. Cao, X. Zhao, *Energy Stor. Mater.* **2019**, *18*, 405.
[39] H. Duan, K. Li, M. Xie, J. M. Chen, H. G. Zhou, X. Wu, G. H. Ning, A. I. Cooper, D. Li, *J. Am. Chem. Soc.* **2021**, *143*, 19446.
[40] X. F. Qiu, H. L. Zhu, J. R. Huang, P. Q. Liao, X. M. Chen, *J. Am. Chem. Soc.* **2021**, *143*, 7242.
[41] Z. Meng, J. Luo, W. Li, K. A. Mirica, *J. Am. Chem. Soc.* **2020**, *142*, 21656.
[42] B. Han, X. Ding, B. Yu, H. Wu, W. Zhou, W. Liu, C. Wei, B. Chen, D. Qi, H. Wang, K. Wang, Y. Chen, B. Chen, J. Jiang, *J. Am. Chem. Soc.* **2021**, *143*, 7104.